Journal of Physics and Chemistry of Solids 142 (2020) 109458

Contents lists available at ScienceDirect

Journal of Physics and Chemistry of Solids

journal homepage: http://www.elsevier.com/locate/jpcs

Modeling of explosives: 1,4,2,3,5,6-dioxatetrazinane as a new green energetic material with enhanced performance

Sergey V. Bondarchuk

Department of Chemistry and Nanomaterials Science, Bogdan Khmelnitsky Cherkasy National University, blvd. Shevchenko 81, 18031, Cherkasy, Ukraine

ARTICLE INFO

Keywords:
Green explosive
Nitrogen-rich solid
High-energy-density material
DFT

ABSTRACT

Crystal structure prediction and characterization data have been computed for two novel carbon-free energetic compounds, namely 1,4,2,3,5,6-dioxatetrazinane (DOTZ) and its 2,5-dinitro derivative (DNDOTZ). Dynamic and mechanical stability of these crystalline materials at ambient pressure has been confirmed. Ab initio molecular dynamics simulations confirmed thermal stability of DOTZ at 298 K and of DNDOTZ at 77 K. A comprehensive spectral characterization (IR, Raman, UV/Vis, NMR) has been performed to provide information for future experimental identification. The parent molecule exhibits powerful detonation properties, which exceed those of most compounds hitherto obtained experimentally or predicted theoretically. Meanwhile, DNDOTZ is predicted to be an effective solid oxidant for common explosives with negative oxygen balance, such as TNT, TNB, DATB, and TATB. Such mixtures demonstrate better propulsive properties than corresponding mixtures of these explosives with gaseous oxygen. By virtue of its zero oxygen balance, the only detonation products of DOTZ are environmentally friendly molecular nitrogen and water. Therefore, this compound is of great potential interest for further energetic applications.

1. Introduction

According to an analysis of the explosives market by Global Industry Analytics, Inc., the global market for explosives is projected to reach 30 million metric tons in 2024 [1]. Since most explosive formulations contain a significant amount of carbon, a huge mass of carbon oxides is released into the atmosphere, exacerbating the greenhouse effect. In this context, carbon-free nitrogen-rich explosives are highly desirable, since these would release environmentally friendly molecular dinitrogen as the primary detonation product. Ideally, pure nitrogen allotropes other than N_2 [2–4] could replace conventional C–H–N–O explosives, but, to date, only three allotropes of nitrogen, both molecular and polymeric (cg-N, LP-N, and N_8), have been characterized experimentally [5–7]. We should stress that these allotropes have been obtained only in very small quantities under extreme conditions; thus, their practical application is still unachievable.

Meanwhile, various H–N–O compounds have attracted close attention due to their superior performances as high-energy-density materials (HEDM). Among these compounds, the family of ammonium salts with various nitrogen-rich carbon-free anions occupies a special place [8–12]. For example, the burning rate of ammonium dinitramide is about 10 times faster than those of ammonium perchlorate, RDX, and HMX [13]. The most widely used cations and anions, as components of these salts, are illustrated in Chart 1. The latter not only have high nitrogen contents, but also display high enthalpies of formation, favorable detonation properties, and remarkable insensitivities [8]. The most promising species among those presented in Chart 1 is the long-sought pentazolate anion *cyclo*-N_5^- [14]. Though this anion was first observed in 2002, its synthesis in the form of an ammonium salt was only reported in 2017 [15,16]. A synthetic route to various salts of the *cyclo*-N_5^- anion has now been developed, making this hitherto elusive species much more readily available [9]. We should stress that the crystal structure of NH_4^+ *cyclo*-N_5^- was predicted earlier using an evolutionary algorithm, and it was calculated that this salt should be thermodynamically stable at pressures above 30 GPa [17]. Despite the wrong space group, the predicted crystalline environment is impressively close to that determined experimentally [9]. This clearly demonstrates the predictive force of modern theoretical methods.

Steele and Oleynik performed an extensive study of ternary C–N–O and H–N–O systems at 50 and 200 GPa using an evolutionary algorithm, and obtained the corresponding phase diagrams [18–21]. A few interesting compounds, namely hydrazinium hydroxide $(N_2H_5)(HO)$–$P2_1/m$, diammonium oxide $(NH_4)_2O$-*Cmcm*, and nitric acid (HNO_3)–$P2_1/m$, were found to be stable at 200 GPa [18]. At 50 GPa, six ternary

E-mail address: bondchem@cdu.edu.ua.

https://doi.org/10.1016/j.jpcs.2020.109458
Received 2 December 2019; Received in revised form 6 March 2020; Accepted 7 March 2020
Available online 10 March 2020
0022-3697/© 2020 Elsevier Ltd. All rights reserved.

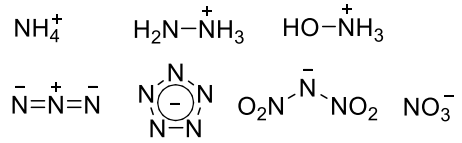

Chart 1. Typical building blocks for carbon-free nitrogen-rich energetic salts.

compounds were located on the convex hull: $H_{10}N_2O$–*C*2/*m*, H_8N_4O-$R\bar{3}m$, HNO_3–$P2_1/m$, $H_6N_2O_8$-$P\bar{1}$, H_8N_2O-$P\bar{3}m1$, and $H_{12}N_2O_3$–*Cm* [18]. Bogdanova et al. [22] calculated detonation parameters of different condensed high explosives of the general composition $H_xN_yO_z$ using a multiphase model of detonation products based on the equations of state.

The aforementioned studies inspired us to model a molecular form of an $H_xN_yO_z$ system having zero oxygen balance $(H_2O)_xN_y$, thus releasing only H_2O and N_2, relatively high nitrogen content (>50 wt%), existing as relatively small molecules, having a high positive enthalpy of formation and crystal density, while maintaining dynamic, mechanical, and thermal stability. Moreover, as we have recently found, the novel energetic polymeric material CarNit4, poly(1,5-tetrazolediyl), demonstrates excellent potential as an explosive, but suffers from a lack of internal oxidant [23]. Thus, we have also modeled a positive oxygen balance material of the composition $H_xN_yO_z$ for potential application as a solid oxidant in explosive formulations or multi-component propellants, alternatives to various heterocyclic compounds [24], or strained nitro-triaziridine derivatives [25–27]. Herein, we present our crystal structure prediction and characterization with respect to dynamic, mechanical, and thermal stability of two crystalline materials, 1, 4,2,3,5,6-dioxatetrazinane (DOTZ) and its 2,5-dinitro derivative (DNDOTZ), as well as information for their future spectral identification.

2. Computational details

The first-principles calculations employed in this work were performed in terms of Density Functional Theory (DFT) within the generalized gradient approximation (GGA) using the Materials Studio 7.0 suite of programs [28]. Geometry optimizations and calculations of band structure (BS), phonons, and vibrational spectra, as well as optical properties and electron excitation energies, were performed with the Cambridge Serial Total Energy Package (CASTEP) code [29]. Elastic constants and lattice energies were obtained using the DMol^3 code [30]. The Perdew–Burke–Ernzerhof (PBE) functional [31] was utilized throughout, except for BS calculations. The latter were performed with a hybrid functional, namely HSE06 [32], which performs better in predicting band gaps than pure GGA functionals [33].

All CASTEP calculations were performed using norm-conserving pseudopotentials (NCP), which accurately describe electron–core interactions. Electronic wave functions were obtained by the density mixing scheme [34] (for PBE) or the preconditioned conjugate gradients method (for HSE06) [35]. These were expanded in a plane wave basis set with an energy cutoff of 830 eV (61.0 Ry). In the DMol^3 calculations, an

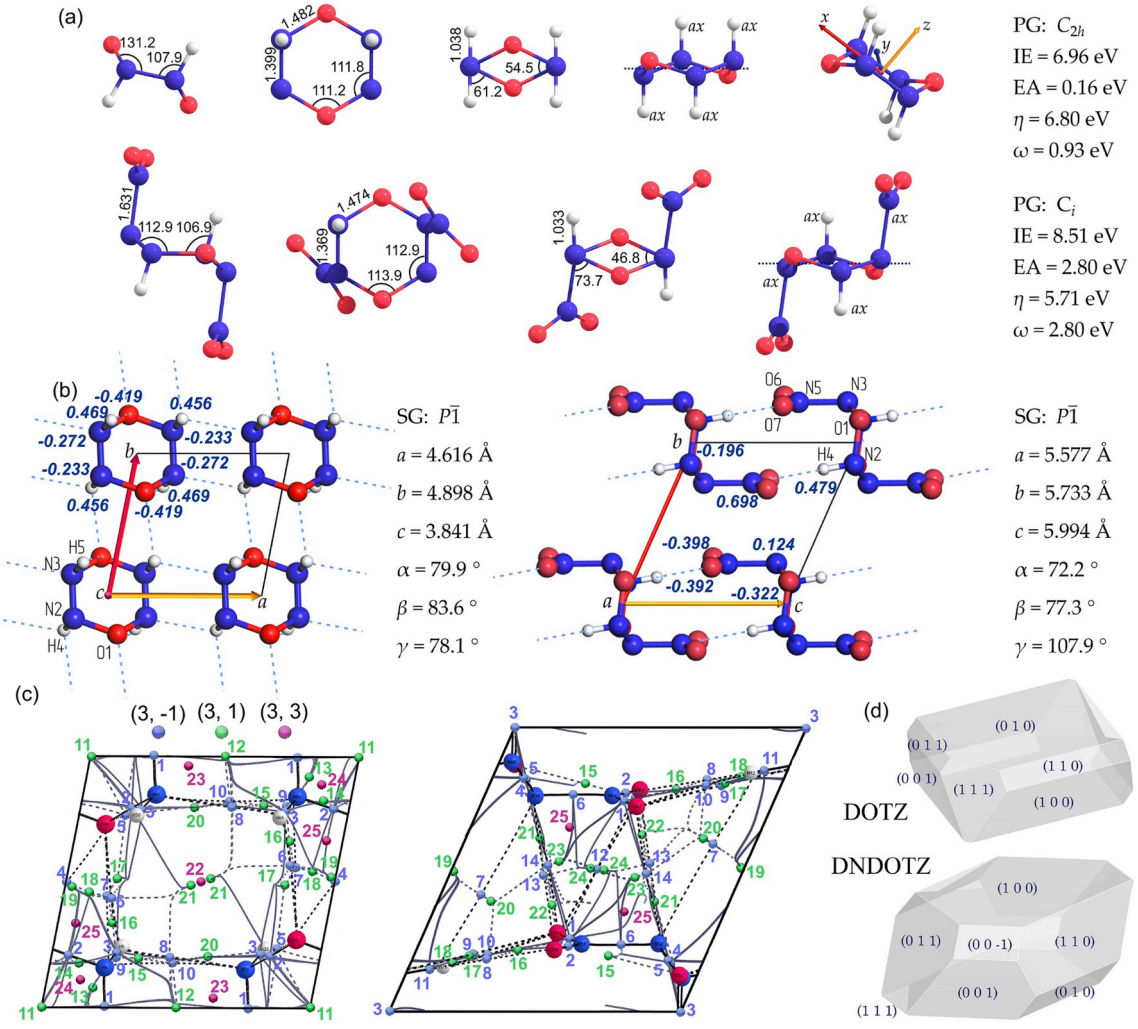

Fig. 1. Structural parameters (a, b), topological analysis (c), and crystal morphologies (d) of the studied H–N–O compounds.

all-electron approximation along with a triple numerical basis set, TNP, was applied [30]. Sampling of the Brillouin zone was performed using a *k*-point grid generated by the Monkhorst–Pack algorithm. Separation of *k*-points was set to 0.05 2πÅ^{-1} for calculations of BS, optical properties, electron transitions, and elastic constants. In all other calculations, the tightness of the *k*-point mesh was set at 0.08 2πÅ^{-1}. Convergence criteria of the total energies were specified as 5×10^{-6} eV atom^{-1} in the SCF calculations and 1×10^{-6} eV atom^{-1} in the fixed geometry calculations. Optimizations of the asymmetric cells were performed by means of the Broyden, Fletcher, Goldfarb, and Shannon (BFGS) method [36]. Long-range effects were fully accounted for (GGA/PBE) using the Grimme form of the damped C_6 term [37]. Time-dependent DFT (TD-DFT) calculations were performed using the Tamm–Dankoff approximation [38].

Topological analysis of the electron density (QTAIM) was performed using wave functions obtained with the projector-augmented-wave-based method (PAW) [39]. These calculations were carried out using the Quantum Espresso 5.3.0 program package [40]. Topological analysis of the electron density was carried out with Critic2 software [41]. Crystal morphology was calculated by the attachment energy method on the basis of crystal graphs. The latter were computed using the COMPASS (Condensed-phase Optimized Molecular Potentials for Atomistic Simulation Studies) forcefield [42] with the Morphology Tools module [28]. The lowest energy at the initial step was set as −2.494 kJ mol^{-1} (thermal energy at room temperature).

Molecular calculations in this work were performed using the Gaussian09 program suite [43]. We applied the DFT/B3LYP [44] method with Pople's split-valence quasi-triple-ζ in the valence shell basis set (6-311G), with the addition of both polarization (2d,2p) and diffuse (++) functions [45].

3. Results and discussion

3.1. Structural features and topological analysis

The structures of the studied compounds (DOTZ and DNDOTZ) in molecular and crystalline forms are illustrated in Fig. 1a and b. In this work, we applied our modified eigenvector-following scheme to find crystal structures (Fig. S1 in the Supplementary data). This method avoids the optimization of a huge number of crystal structures, which are often very odd or improbable (as with purely automatic algorithms), and restrict the number of structures to just a few. Obviously, one can never be 100% sure that the predicted structure is a real Nature-created crystal, but the fact that a crystal structure (probably a metastable polymorph) can be accessed under the given conditions means that a stable form of this compound does definitely exist. On the other hand, for the majority of organic crystals, energy separation between polymorphs does not exceed 2 kJ mol^{-1}, and the difference between their densities is of the order of 0–2% [46]. Recently, we obtained a similar result in the crystal structure prediction of benzenediazonium chloride using the Polymorph predictor [47].

The modeled compounds, DOTZ and DNDOTZ, belong to the C_{2h} and C_i symmetry point groups, respectively. According to our algorithm, these molecules were pasted into the constructed cells such that their inversion centers were aligned with the high-symmetry point (0,0,0). After symmetrization, the resulting space group was $P\bar{1}$ and the corresponding Z' values became 1/2. This packing mode is in complete accordance with the known empirical rules for molecular crystals [48]. The crystals obtained in this way appeared to be well stabilized by hydrogen bonds, showed a uniform filling of the space, and had good densities (see Fig. S2 in the Supplementary data). Increasing Z' to 1 led to the higher-energy structures, as was proven by corresponding calculations with two popular predictors, namely USPEX [49] and Polymorph [28].

The optimized asymmetric cell parameters along with the structural

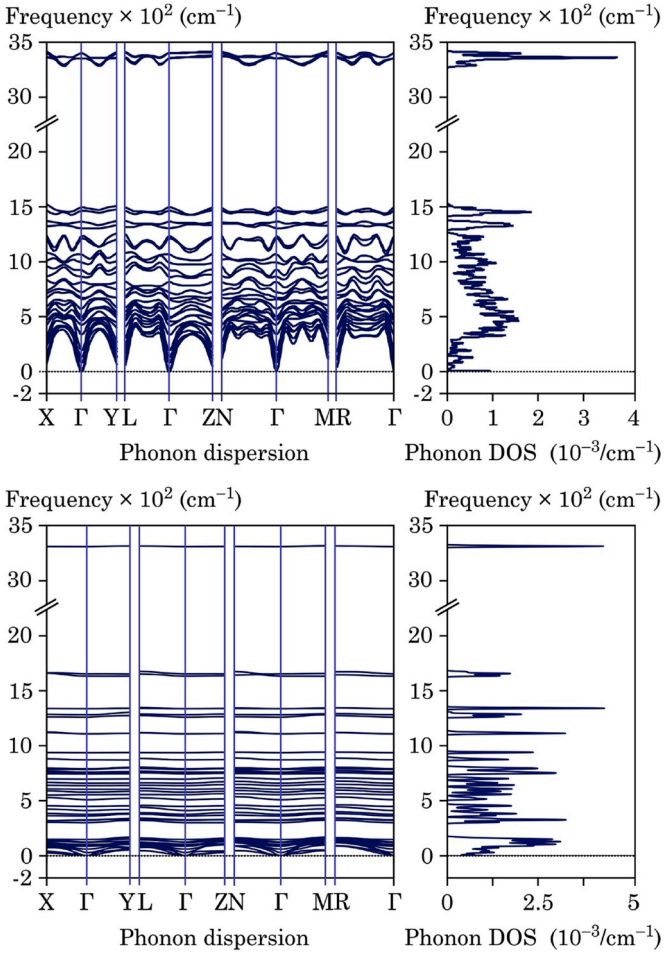

Fig. 2. Plots of phonon dispersion and density of phonon states for DOTZ (top) and DNDOTZ (bottom).

features of DOTZ and DNDOTZ are illustrated in Fig. 1. Bond lengths, angles, and Bader charges are given in angstroms, degrees, and parts of electronic charges, respectively. According to Fig. 1, the studied compounds appear to be armchair conformers with *a*,*a*,*a*,*a* positions of the hydrogen atoms; this conformer was found to be the most energetically preferable in the crystalline environment.

The values of electrophilicity index (ω) [50] were calculated using the following expression:

$$\varpi = \frac{(IE + EA)^2}{8(IE - EA)} \quad (1)$$

where $IE = -E_{HOMO}$ and $EA = -E_{LUMO}$ (E_{HOMO} and E_{LUMO} are the energies of the highest occupied and lowest unoccupied molecular orbitals, respectively). In Fig. 1, $\eta = IE - EA$, corresponding to chemical hardness [50]. According to the ω values, DOTZ has nucleophilic rather than electrophilic character, whereas DNDOTZ is rendered a strong electrophile by the influence of the two NO_2 groups.

QTAIM analysis of a crystal of DOTZ revealed the presence of O···H and N···H hydrogen bonds. Numerical data on electron density and its derivatives at all of the located critical points (CPs) are listed in Table S1 in the Supplementary data. The crystal is additionally stabilized through van der Waals contacts O···O (CP4), N···O (CP7), and N···N (CP10). According to the Cremer–Kraka criterion ($\nabla^2\rho(\mathbf{r}) > 0$, $K(\mathbf{r}) < 0$), these are weak, closed-shell interactions [51]. A similar picture was found in the case of the DNDOTZ crystal (Fig. 1c). In this case, however, some hydrogen bonds were not detected automatically by estimating the closest interatomic distances between hydrogen atoms and heteroatoms

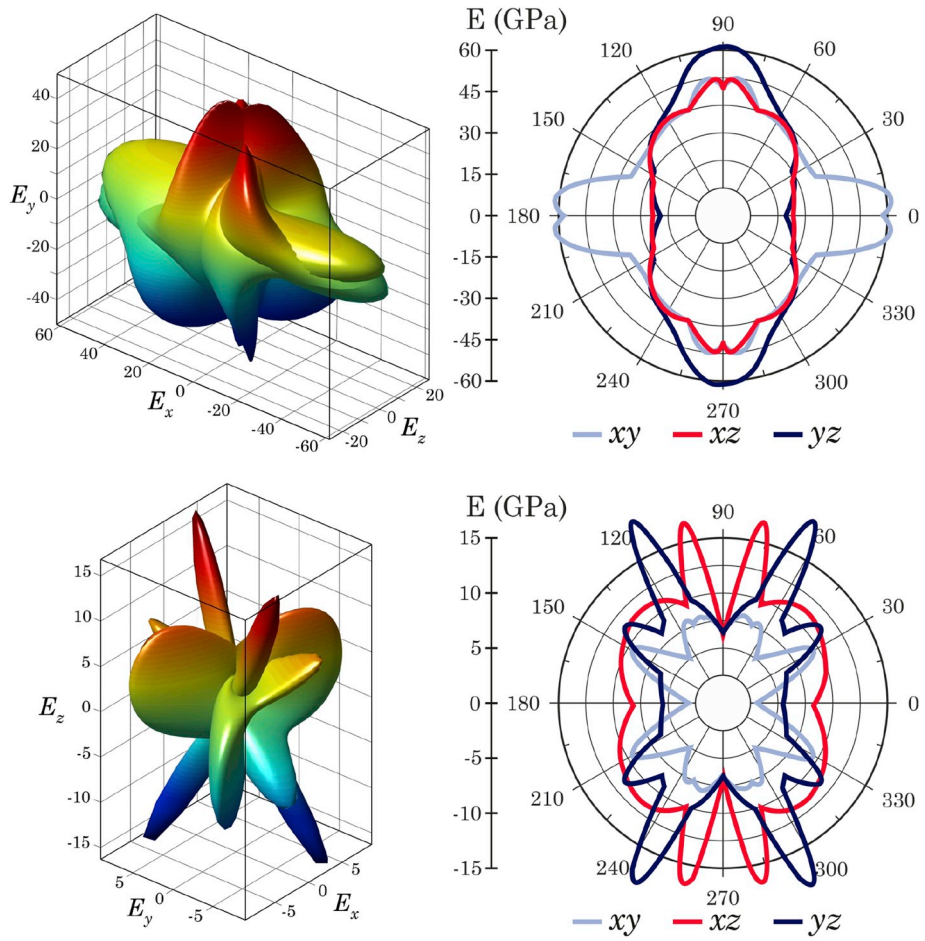

Fig. 3. Graphical representation of the Young's modulus for DOTZ (top) and DNDOTZ (bottom).

(Fig. 1b). This proves the need for topological analysis of the electron density distribution, whereby all interactions within an asymmetric cell can be found. Thus, weak hydrogen bonds (CP7) and van der Waals contacts O···O (CP10 and 12), N···O (CP13 and 14) were also found; however, N···N contacts are absent in the DNDOTZ crystal (Table S1 in the Supplementary data).

We also calculated crystal growth morphologies in vacuo, and the obtained crystal habits, with the stable faces indicated, are illustrated in Fig. 1d. Corresponding numerical data, including relative areas of the stable faces and growth slice thicknesses, d_{hkl}, are listed in Table S2 in the Supplementary data. On the basis of crystal habits, an important parameter, namely sphericity (Ψ), was calculated for DOTZ and DNDOTZ as 1.268 and 1.231, respectively. Recently, we have shown that Ψ values are directly proportional to impact energy [52–55]. In the case of a strong dependence between crystal habit sphericity and impact sensitivity, the latter can be easily tuned by altering the crystallization conditions. Considering the Ψ values for DOTZ and DNDOTZ, the latter is expected to be more sensitive to impact.

3.2. Stability criteria

In our crystal structure prediction scheme, all of the relaxed structures were checked for the absence of imaginary frequencies at the Γ-point (NIMAG = 0). However, since the absence of imaginary modes at the Γ-point does not guarantee dynamic stability of the structure, all of the crystals with NIMAG = 0 were further checked for the absence of soft modes within the entire Brillouin zone. The obtained plots of phonon dispersion and density of phonon states are illustrated in Fig. 2. Integration of the Brillouin zone was performed according to the standardized approach (high-throughput approximation) for integration of all 24 Brillouin zones [56]. The coordinates of the high-symmetry points are listed in Table S3 in the Supplementary data. As one can see in Fig. 2, the studied crystals are characterized by an absence of soft modes. Acoustic branches demonstrate linearity near the Γ-point. The N–N and N–O valence vibrational frequencies are about 1500 cm^{-1}, indicating good mechanical strength of these bonds.

Further, we checked the mechanical stabilities of DOTZ and DNDOTZ. Actually, for such low-symmetry crystals (triclinic, $P\bar{1}$), the corresponding necessary and sufficient condition of the mechanical stability is that the elastic stiffness constant matrix A_{ij} is positive definite [57]. Mathematically, this condition can be checked using the theorem stating that to be positive definite it is necessary and sufficient that the six leading principal minors of the matrix A_{ij} are all positive (Eq. (2)):

$$\det M_i > 0, i = 1, \ldots, 6 \quad (2)$$

where M_i are six principal minors of the elastic stiffness matrix A_{ij}. Note that $M_6 = \det A_{ij}$.

The studied triclinic crystal systems have 21 independent elastic stiffness (C_{ij}) and compliance ($S_{ij} = 1/C_{ij}$) constants. The calculated values are listed in Tables S4 and S5 in the Supplementary data. As one can easily check, DOTZ and DNDOTZ are both mechanically stable crystals. They are characterized by very strong anisotropy of the Young's modulus (Fig. 3), which, in some directions, reaches about 40 and 15 GPa for DOTZ and DNDOTZ, respectively. The crystals represent relatively soft matter, with estimated bulk moduli of 28.6 and 9.5 GPa for DOTZ and DNDOTZ, respectively. Numerical data on the Young's moduli and Poisson's ratios are gathered in Table 1.

To determine the thermal stability range, we performed *ab initio*

Table 1
Calculated Young's moduli (E, GPa) and Poisson ratios (ν) of the studied materials.

Axis	E (GPa)		Poisson Ratios (ν)					
	DOTZ	DNDOTZ		DOTZ	DNDOTZ		DOTZ	DNDOTZ
x	57.71	1.4934	E_{xy}	−0.1585	0.6466	E_{xz}	0.5680	0.2846
y	37.99	2.0902	E_{yx}	−0.1043	0.9050	E_{yz}	0.7267	0.0834
z	22.87	3.5254	E_{zx}	0.2250	0.6718	E_{zy}	0.4374	0.1407

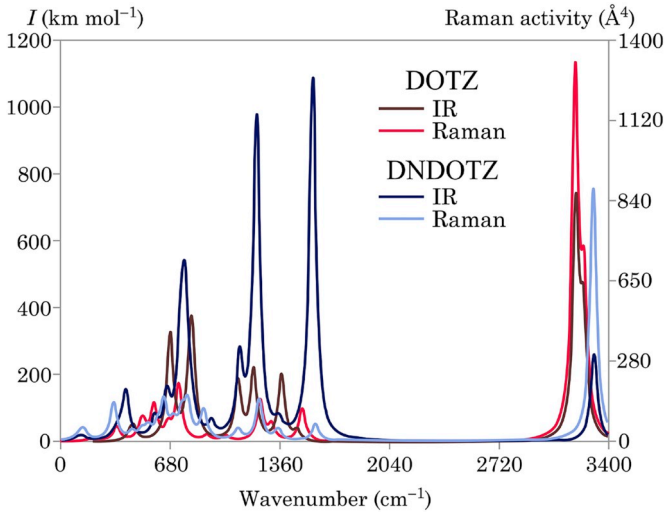

Fig. 4. Calculated IR and Raman spectra (bandwidth at half-height: 50 cm^{-1}).

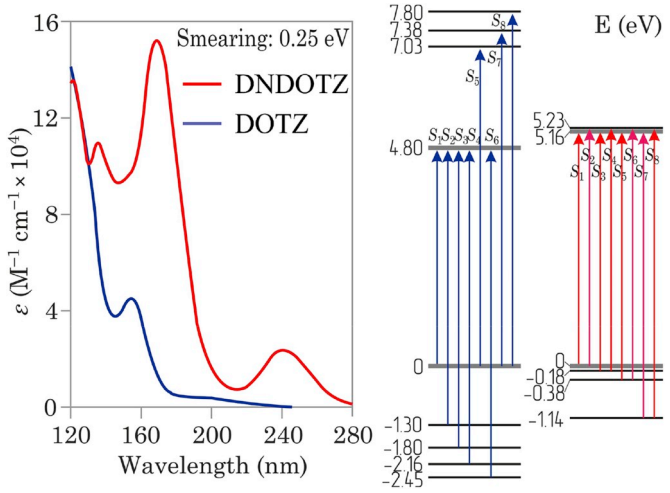

Fig. 5. Calculated absorption spectra and descriptions of the first eight electronic transitions.

molecular dynamics simulations within a 5 ps timescale (time step 1 fs) using a supercell with two molecules. The simulations were performed with the NVT ensemble by the PBE/DND approach, as implemented in the DMol^3 code [30]. DOTZ was found to be thermally stable at 298 K, with DNDOTZ being stable at around 77 K. At higher temperatures, the latter compound decomposes into NO_2, NO, HONO, HN_2, and so on. Thus, DOTZ should be accessible under ambient conditions and may be used as a conventional energetic material, while DNDOTZ may only be stored at liquid nitrogen temperature.

3.3. Spectral data

We performed a series of calculations on the spectral properties of DOTZ and DNDOTZ to aid their future experimental identification, as well as for estimation of their thermodynamic properties. The calculated infra-red (IR) and Raman spectra are plotted in Fig. 4, and the numerical data, along with the eigenvectors of the vibrational modes, are presented in Table S6 and Figs. S3 and S4 in the Supplementary data.

Due to the nonplanar shape of the molecules, it is difficult to assign individual vibrations, which are often mutual and include bond stretching (ν), in-plane (δ) and out-of-plane (γ) deformations. All of the IR-intense and Raman-active vibrations in the spectrum of DOTZ are γ_{N-H} and ν_{N-H} (Table S6 and Fig. S3 in the Supplementary data). The IR spectrum of DNDOTZ is similar, but with some additional intense δ_{NO_2} bands (1560, 1212, and 769 cm^{-1}).

Plots of BS and partial density of states (PDOS) are illustrated in Fig. S5 in the Supplementary data. According to these plots, DOTZ and DNDOTZ are both insulators, with band gaps of 5.384 and 4.816 eV, respectively. Moreover, we calculated the optical properties of the studied materials. Their absorption spectra are illustrated in Fig. 5, and their other properties (reflectivity, refractive index, dielectric function, conductivity, and loss function) are presented in Fig. S6 in the Supplementary data. To elucidate the nature of the absorption spectra, we calculated the first eight electronic transitions using TD-DFT (Fig. 5).

Due to the indirect band gap of DOTZ, the first vertical transition occurs from VB–1 to CB (VB and CB denote the valence band and conduction band, respectively). This corresponds to the first absorption band with λ_{max} = 200 nm (Fig. 5). Note that frontier crystal orbitals, which are involved in these electron transitions, are illustrated in Fig. S7 in the Supplementary data. In the case of DNDOTZ, the band gap is direct and CB and CB+1 are close-lying, as are VB, VB–1, and VB–2 (Fig. 5). As a result, the first six electronic transitions form a much more intense band with λ_{max} = 240 nm and ε = 23600 M^{-1} cm^{-1}, as compared with 3800 M^{-1} cm^{-1} in the case of DOTZ (Fig. 5). Thus, the studied materials are expected to be transparent solids.

Finally, we calculated nuclear magnetic resonance (NMR) and electric field gradient (EFG) properties (Table S7 in the Supplementary data). If synthesized, we hope that the collected spectral data will help experimentalists to identify the studied compounds.

3.4. Detonation, thermodynamic, and propulsive properties

To estimate the detonation properties of the studied compounds, we calculated their solid-state enthalpies of formation (ΔH^0_{solid}) according to Eq. (3) [58]:

$$\Delta H^0_{solid} = \Delta H^0_{gas} - \Delta H_{sub} \quad (3)$$

where ΔH^0_{gas} is the gas-phase enthalpy of formation and ΔH_{sub} is the sublimation energy. In turn, the gas-phase enthalpies of formation were calculated according to Eq. (4):

$$\Delta H^0_{gas} = E_{H_iN_jO_k} - (iE_H + jE_N + kE_O) \quad (4)$$

where $E_{H_iN_jO_k}$ and E_X are the zero-point energy (ZPE)-corrected total energies of the given molecule and the constituent elements in their stationary states ($^1\Sigma_g^+$ H_2, $^1\Sigma_g^+$ N_2, and $^3\Sigma_g^-$ O_2). In this work, we slightly modified the B3LYP/6–311++G(2d,2p) energies of the H, N, and O atoms in order to better reproduce the known enthalpies of formation for different $H_xN_yO_z$ molecules. The final energies were evaluated as E_H =

Table 2
Calculated enthalpies of formation (kJ mol^{-1}).

Phase	ΔH^0_{gas}	ΔH_{sub}	ΔH^0_{solid}
DOTZ	422.8	157.1	265.7
DNDOTZ	526.4	115.9	410.5

−0.58498, E_N = −54.77927, and E_O = −75.18198 Eh/atom. Substituting ΔH_{sub} in Eq. (3) in its form of the lattice energy (E_{latt}) expression, one obtains Eq. (5):

$$\Delta H^0_{solid} = \Delta H^0_{gas} + \frac{E_{solid}}{Z} - E_{gas} + 2RT \quad (5)$$

Here, $1/Z\ E_{solid} - E_{gas} = E_{latt}$ and $-E_{latt} - 2RT = \Delta H_{sub}$.

The calculated ΔH^0_{solid} values are gathered in Table 2. It can be seen that the studied compounds have high enthalpies of formation, being much more energy-dense than conventional explosives (RDX, HMX, TATB, etc.) [59]. The obtained enthalpies of formation along with the crystal densities (Table 3) were used within the Kamlet–Jacobs (K-J) empirical scheme for prediction of detonation energy (Q), velocity (D), and pressure (P) [60]. Recently, we found that the K-J scheme outperforms the most recent predictors (EMDB, EXPLO5, and Cheetah 8.0) in terms of accuracy in the estimation of detonation velocity [61].

Both compounds studied in this work have high internal oxidation abilities. The corresponding structural criterion used for the K-J calculations [60] is presented in Table 3. The N, $\overline{M}$, and Q values were calculated according to Eqs. (6) and (7):

$$N = \frac{1}{\overline{M}} = \frac{b + 2c + 2d}{4MW} \quad (6)$$

$$Q = \frac{28.9b + 94.05a + 239\Delta H^0_f}{MW} \quad (7)$$

Here, a, b, c, and d denote the numbers of carbon, hydrogen, nitrogen, and oxygen atoms, respectively, and MW is the molecular weight. The calculated values of Q, D, and P are listed in Table 3. It can be seen that DOTZ demonstrates enhanced theoretical detonation performance compared to all of the known conventional explosives. The only exceptions are single-bonded nitrogen allotropes, but these materials are either not synthetically accessible at all [2,3] or are not available in sufficient quantities [5–7]. In comparison, DNDOTZ exhibits smaller values of Q, D, and P, which may be attributed to its high positive oxygen balance (43.9%). Thus, the use of DNDOTZ as a pure explosive agent would not be appropriate, whereas DOTZ might be applied as a single-component powerful green explosive.

In addition to their detonation properties, we estimated the propulsive characteristics of the studied compounds. Considering the vibrational spectra with no imaginary frequencies (Table S6 in the Supplementary data), we obtained the thermodynamic properties of the studied crystalline materials. The temperature dependences of the main thermodynamic functions are presented graphically in Fig. 6. These data were then converted into the NASA 9-coefficient form through simultaneous fitting of the following three polynomials [62]:

$$\frac{C^\circ_p}{R} = a_1T^{-2} + a_2T^{-1} + a_3 + a_4T + a_5T^2 + a_6T^3 + a_7T^4 \quad (8)$$

$$\frac{H^\circ}{RT} = -a_1T^{-2} + a_2T^{-1} + \ln T + a_3 + a_4\frac{T}{2} + a_5\frac{T^2}{3} + a_6\frac{T^3}{4} + a_7\frac{T^4}{5} + \frac{a_8}{T} \quad (9)$$

$$\frac{S^\circ}{R} = -a_1\frac{T^{-2}}{2} - a_2T^{-1} + a_3\ln T + a_4T + a_5\frac{T^2}{2} + a_6\frac{T^3}{3} + a_7\frac{T^4}{4} + a_9 \quad (10)$$

The obtained coefficients for DOTZ and DNDOTZ are presented in formatted view in the Supplementary data.

These data were then applied to calculate the propulsive properties of DOTZ and DNDOTZ as pure propellants and in mixtures with other components. The calculations were performed in the framework of the finite-area combustion chamber approximation using the NASA CEA program [63]. Since both compounds studied in this work have a sufficient amount of internal oxidant (O) with respect to the fuel (H), there is no need to mix them with an external oxidant. On the contrary, DNDOTZ has an oxygen balance of 43.9% and may itself be applied as an oxidant. The calculated propulsive properties of DOTZ and DNDOTZ as monopropellants, specifically combustion chamber temperature (*CCT*, K), average molecular weight of exhaust gas (M, 1/n), specific impulse (I_{sp}, s), vacuum specific impulse (I_{vac}, s), and characteristic velocity (c^*, m/s), are listed in Table 4. Note that O/F denotes the oxidant-to-fuel weight ratio.

According to the data in Table 4, DOTZ demonstrates enhanced propulsive properties compared to conventional explosives such as RDX (I_{sp} = 268 s) [64]. At the same time, DNDOTZ demonstrates inferior performance because of its significant positive oxygen balance. Therefore, we calculated the propulsive properties of mixtures of DNDOTZ with various common explosives having negative oxygen balance. The latter were also mixed with gaseous oxygen as an external oxidant to compare the effectiveness of O_2 and DNDOTZ. The obtained results are listed in Table 5.

The calculations revealed complex chemical compositions of the detonation products in different zones of the combustor. These zones are usually divided according to different exit-to-throat area ratios (Ae/At), namely chamber, throat (Ae/At = 1), and exit (Ae/At = 10, 25, 50, and 68.9). Maximum performance was observed in the case of a simultaneous oxidation to CO and CO_2. Neither CO nor CO_2 can be a single oxidation product of the carbon atoms. In both cases, the propulsive properties decrease. The mole fractions of detonation products at

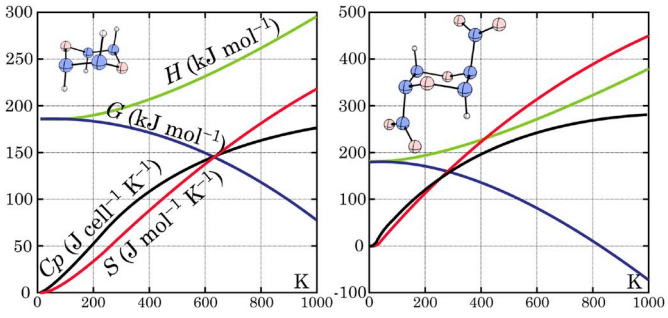

Fig. 6. Temperature dependences of the main thermodynamic functions.

Table 4
Calculated propulsive properties of the studied compounds as monopropellants (O/F = 0).

Species	*CCT*	M	I_{sp}	I_{vac}	c^*
DOTZ	3078	22.3	297.9	326.6	1779.9
DNDOTZ	2658	28.0	230.9	246.6	1400.5

Table 3
Calculated detonation properties, structural criteria, nitrogen contents (N), and oxygen balances Ω_{CO_2}.

Crystal	Structural criterion	N (wt%)	Ω_{CO_2} (%)	ρ (g cm^{-3})	Q (cal g^{-1})	D (km s^{-1})	P (GPa)
DOTZ	$d \geq 2a + b/2$	60.9	0	1.834	1945.5	10.4	48.2
DNDOTZ	$d \geq 2a + b/2$	46.2	43.9	1.857	856.4	8.1	29.7

Table 5
Calculated propulsive properties for mixtures of negative oxygen balance explosives with DNDOTZ (Ox1) and O_2 (Ox2) as oxidants.

Species	O/F		*CCT*		*M*		I_{sp}		I_{vac}		c^*	
	Ox1	Ox2	Ox1	Ox2	Ox1	Ox2	Ox1	Ox2	Ox1	Ox2	Ox1	Ox2
TNT	0.795	0.345	3099	3085	27.2	27.7	268.8	264.8	292.8	287.9	1604.1	1580.1
TNB	0.585	0.225	3113	3098	28.6	29.0	263.7	259.6	288.2	282.3	1573.3	1549.0
DATB	0.655	0.285	3041	3018	27.7	28.4	263.7	258.9	287.3	281.6	1572.5	1543.7
TATB	0.675	0.295	3029	3006	27.2	27.9	265.0	260.4	288.4	283.4	1580.3	1552.9

different Ae/At ratios are listed in Table S8 in the Supplementary data. As can be seen in Table S8, a trace amount of hydrogen gas was present; however, it did not exceed a mole fraction of 0.12. A simple increase in the relative amount of oxidant led to an increase in the CO_2/CO ratio, not the oxidation of H_2, and, as we have mentioned above, this does not improve the propulsive characteristics.

As one can see in Table 5, DNDOTZ is a more effective oxidant than gaseous O_2; thus, mixing of negative oxygen balance explosives (those listed in Table 5, and other similar compounds) with DNDOTZ significantly improves their propulsive properties compared to when they are used alone (Table S9 in the Supplementary data).

4. Conclusions

In summary, the presented results reveal that DOTZ and DNDOTZ are stable in the crystalline state (with space group $P\bar{1}$). This was corroborated by corresponding calculations of phonon dispersions and elastic constants as well as molecular dynamics simulations. DOTZ exhibits excellent detonation properties and outperforms all hitherto known explosives, both those obtained experimentally and those predicted theoretically. In comparison, DNDOTZ shows inferior detonation performance, mainly due to a strong imbalance between the internal oxidant (O) content and the reductant (H) content, leading to a large positive oxygen balance (43.9%). However, the use of this compound as an external oxidant may significantly improve the propulsive properties (and obviously the detonation properties too) of common explosives with a high negative oxygen balance (TNT, TNB, DATB, TATB). Indeed, mixtures of DNDOTZ with the latter show higher propulsive characteristics than the corresponding mixtures with O_2 as an external oxidant.

To provide experimentalists with some guidance for construction of the DOTZ ring, we cite papers on the synthesis of oxazinane and dioxadiazine rings [65–67]. We hope that this will expedite the development of an appropriate synthetic protocol. The issue of the sensitivities of DOTZ and DNDOTZ will be addressed in a separate study. Electrostatic potential (ESP) on the molecular surface can rationalize intermolecular interactions and predict chemically reactive sites. At first glance, one can assume relatively high impact sensitivity of DOTZ, which should be comparable to that of triacetone triperoxide (TATP). This is primarily caused by the strongly electron-deficient ring of DOTZ. Our calculations of decomposition activation energy of DOTZ in the gas phase yielded a value of 98.4 kJ mol^{-1} (Fig. S8 in the Supplementary data). Considering the corresponding value for TATP (131.1 kJ mol^{-1}) [68], the impact sensitivity of DOTZ can be expected to be about 75% of that of TATP.

A good method for increasing the stability of an energetic material is to convert it into a salt. The most obvious type of salts that might be derived from these structures are of the ammonium type. However, protonation at the nitrogen atoms of DOTZ is unlikely due to the presence of the electron-accepting oxygen atoms. Thus, the structure of hexazinane (oxygen atoms replaced by NH) as a proton acceptor is of great interest. Combination of a hexazinanium cation with the anions in Chart 1 may afford very powerful and stable green explosives, which will be the subject of further studies.

Declaration of competing interest

The authors declare that they have no known competing financial interests or personal relationships that could have appeared to influence the work reported in this paper.

CRediT authorship contribution statement

Sergey V. Bondarchuk: Conceptualization, Methodology, Software, Data curation, Writing - original draft, Visualization, Investigation, Writing - review & editing.

Acknowledgments

This work was supported by the Ministry of Education and Science of Ukraine Research Fund (Grant No. 0118U003862).

Appendix A. Supplementary data

Supplementary data to this article can be found online at https://doi.org/10.1016/j.jpcs.2020.109458.

References

[1] Explosives – market analysis, trends and forecasts. https://www.strategyr.com/market-report-explosives-forecasts-global-industry-analysts-inc.asp. (Accessed 5 November 2019).
[2] S.V. Bondarchuk, Beyond molecular nitrogen: revelation of two ambient-pressure metastable single- and double-bonded nitrogen allotropes built from three-membered rings, Phys. Chem. Chem. Phys. 21 (2019) 22930–22938.
[3] S.V. Bondarchuk, B.F. Minaev, Super high-energy density single-bonded trigonal nitrogen allotrope—a chemical twin of the cubic gauche form of nitrogen, Phys. Chem. Chem. Phys. 19 (2017) 6698–6706.
[4] S.V. Bondarchuk, B.F. Minaev, Two-dimensional honeycomb (A7) and zigzag sheet (ZS) type nitrogen monolayers. A first principles study of structural, electronic, spectral, and mechanical properties, Comput, Mater. Sci. 133 (2017) 122–129.
[5] M.I. Eremets, A.G. Gavriliuk, I.A. Trojan, D.A. Dzivenko, R. Boehler, Single-bonded cubic form of nitrogen, Nat. Mater. 3 (2004) 558–563.
[6] D. Tomasino, M. Kim, J. Smith, C.-S. Yoo, Pressure-induced symmetry-lowering transition in dense nitrogen to layered polymeric nitrogen (LP-N) with colossal Raman intensity, Phys. Rev. Lett. 113 (2014), 205502.
[7] S. Duwal, Y.-J. Ryu, M. Kim, C.-S. Yoo, S. Bang, K. Kim, N. Hwi Hur, Transformation of hydrazinium azide to molecular N_8 at 40 GPa, J. Chem. Phys. 148 (2018), 134310.
[8] G. Zhao, D. Kumar, L. Hu, J.M. Shreeve, A safe and scaled up route to inert ammonia oxide hydroxylammonium azide ($H_7N_5O_2$), hydrazinium azide (H_5N_5) and ammonium azide (H_4N_4), ACS Appl. Energy Mater. 2 (2019) 6919–6923.
[9] Y. Xu, L. Tian, D. Li, P. Wang, M. Lu, A series of energetic cyclo-pentazolate salts: rapid synthesis, characterization, and promising performance, J. Mater. Chem. A 7 (2019) 12468–12479.
[10] C. Yang, C. Zhang, Z. Zheng, C. Jiang, J. Luo, Y. Du, B. Hu, C. Sun, K.O. Christe, Synthesis and characterization of cyclo-pentazolate salts of NH_4^+, NH_3OH^+, $N_2H_5^+$, $C(NH_2)_3^+$, and $N(CH_3)_4^+$, J. Am. Chem. Soc. 140 (2018) 16488–16494.
[11] R. Gilardi, R.J. Butcher, A new class of flexible energetic salts, part 6: the structures of the hydrazinium and hydroxylammonium salts of dinitramide, J. Chem. Crystallogr. 30 (2000) 599–604.
[12] J.C. Bottaro, P.E. Penwell, R.J. Schmitt, 1,1,3,3-Tetraoxo-1,2,3-triazapropene anion, a new oxy anion of nitrogen: the dinitramide anion and its salts, J. Am. Chem. Soc. 119 (1997) 9405–9410.
[13] P. Thakre, Y. Duan, V. Yang, Modeling of ammonium dinitramide (ADN) monopropellant combustion with coupled condensed and gas phase kinetics, Combust. Flame 161 (2014) 347–362.
[14] K.O. Christe, Recent advances in the chemistry of N_5^+, N_5^- and high-oxygen compounds, Propellants, Explos. Pyrotech. 32 (2007) 194–204.
[15] Ch Zhang, Ch Sun, B. Hu, Ch Yu, M. Lu, Synthesis and characterization of the pentazolate anion *cyclo*-N_5^- in $(N_5)_6(H_3O)_3(NH_4)_4Cl$, Science 355 (2017) 374–376.
[16] Y. Xu, Q. Wang, C. Shen, Q. Lin, P. Wang, M. Lu, A series of energetic metal pentazolate hydrates, Nature 549 (2017) 78–81.
[17] B.A. Steele, I.I. Oleynik, Pentazole and ammonium pentazolate: crystalline hydronitrogens at high pressure, J. Phys. Chem. A 121 (2017) 1808–1813.

[18] B.A. Steele, Computational Discovery of Energetic Polynitrogen Compounds at High Pressure, Ph.D. Dissertation, University of South Florida, Tampa, FL, 2018.
[19] B.A. Steele, I.I. Oleynik, Computational discovery of new high-nitrogen energetic materials, in: N. Goldman (Ed.), Computational Approaches for Chemistry under Extreme Conditions, Springer, Cham, 2019, pp. 25–52.
[20] B.A. Steele, I.I. Oleynik, New phase of ammonium nitrate: a monoclinic distortion of AN-IV, J. Chem. Phys. 143 (2015) 234705.
[21] B.A. Steele, I.I. Oleynik, Ternary inorganic compounds containing carbon, nitrogen, and oxygen at high pressures, Inorg. Chem. 56 (2017) 13321–13328.
[22] YuA. Bogdanova, S.A. Gubin, A.A. Anikeev, S.B. Victorov, Thermodynamic modelling of detonation H-N-O high explosives, J. Phys.: Conf. Ser. 751 (2016), 012018.
[23] S.V. Bondarchuk, CarNit4 – A New Polymeric Energetic Material Based on Poly (1,5-Tetrazolediyl), Polymer, accepted manuscript.
[24] T.S. Hermann, Investigation of Oxygen- and Nitrogen-Rich Heterocyclic Compounds as Potential High-Energy Dense Oxidizers or Secondary Explosives, Ph. D. Dissertation, Ludwig Maximilian University, Munich, 2018.
[25] W. Chi, B. Li, H. Wu, Density functional theory study on energetic nitro-triaziridine derivatives, Struct. Chem. 24 (2013) 375–381.
[26] R. Peverati, J.S. Siegel, K.K. Baldridge, Ab initio quantum chemical computations of substituent effects on triaziridine strain energy and heat of formation, Phys. Chem. Chem. Phys. 11 (2009) 2387–2395.
[27] A. Karahodza, K.J. Knaus, D.W. Ball, Cyclic triamines as potential high energy materials. Thermochemical properties of triaziridine and triazirine, J. Mol. Struct.: THEOCHEM 732 (2005) 47–53.
[28] Materials Studio 7.0, Accelrys, Inc., San Diego, CA, 2013.
[29] S.J. Clark, M.D. Segall, C.J. Pickard, P.J. Hasnip, M.J. Probert, K. Refson, M. C. Payne, First principles methods using CASTEP, Z. für Kristallogr. - Cryst. Mater. 220 (2005) 567–570.
[30] B. Delley, From molecules to solids with the DMol^3 approach, J. Chem. Phys. 113 (2000) 7756–7764.
[31] J.P. Perdew, K. Burke, M. Ernzerhof, Generalized gradient approximation made simple, Phys. Rev. Lett. 77 (1996) 3865–3868.
[32] J. Heyd, G. Scuseria, Efficient hybrid density functional calculations in solids: assessment of the Heyd-Scuseria-Ernzerhof screened Coulomb hybrid functional, J. Chem. Phys. 121 (2004) 1187–1192.
[33] A.J. Garza, G.E. Scuseria, Predicting band gaps with hybrid density functionals, J. Phys. Chem. Lett. 7 (2016) 4165–4170.
[34] G. Kresse, J. Furthmüller, Efficient iterative schemes for ab initio total-energy calculations using a plane-wave basis set, Phys. Rev. B 54 (1996) 11169–11186.
[35] M.C. Payne, M.P. Teter, D.C. Allan, T.A. Arias, J.D. Joannopoulos, Iterative minimization techniques for ab initio total-energy calculations: molecular dynamics and conjugate gradients, Rev. Mod. Phys. 64 (1992) 1045–1097.
[36] R. Fletcher, Practical Methods of Optimization, vol. 1, Wiley, New York, 1980.
[37] S. Grimme, Semiempirical GGA-type density functional constructed with a long-range dispersion correction, J. Comput. Chem. 27 (2006) 1787–1799.
[38] S. Hirata, M. Head-Gordon, Time-dependent density functional theory within the Tamm-Dancoff approximation, Chem. Phys. Lett. 314 (1999) 291–299.
[39] G. Kresse, D. Joubert, From ultrasoft pseudopotentials to the projector augmented-wave method, Phys. Rev. B 59 (1999) 1758–1775.
[40] P. Giannozzi, S. Baroni, N. Bonini, M. Calandra, R. Car, C. Cavazzoni, D. Ceresoli, G.L. Chiarotti, M. Cococcioni, I. Dabo, A. Dal Corso, S. Fabris, G. Fratesi, S. de Gironcoli, R. Gebauer, U. Gerstmann, C. Gougoussis, A. Kokalj, M. Lazzeri, L. Martin-Samos, N. Marzari, F. Mauri, R. Mazzarello, S. Paolini, A. Pasquarello, L. Paulatto, C. Sbraccia, S. Scandolo, G. Sclauzero, A.P. Seitsonen, A. Smogunov, P. Umari, R.M. Wentzcovitch, J. Phys. Condens. Matter 21 (2009), 395502.
[41] A. Otero-De-La-Roza, E.R. Johnson, V. Luaña, Critic2: a program for real-space analysis of quantum chemical interactions in solids, Comput. Phys. Commun. 185 (2014) 1007–1018.
[42] H. Sun, COMPASS: an ab initio force-field optimized for condensed-phase applications overview with details on alkane and benzene compounds, J. Phys. Chem. B 102 (1998) 7338–7364.
[43] M.J. Frisch, G.W. Trucks, H.B. Schlegel, G.E. Scuseria, M.A. Robb, J.R. Cheeseman, G. Scalmani, V. Barone, B. Mennucci, G.A. Petersson, et al., Gaussian 09, Revision A.02, Gaussian, Inc., Wallingford, CT, 2009.
[44] A.D. Becke, Density-functional thermochemistry. III. The role of exact exchange, J. Chem. Phys. 98 (1993) 5648–5652.
[45] W.J. Hehre, L. Radom, P.v.R. Schleyer, J.A. Pople, Ab Initio Molecular Orbital Theory, Wiley, New York, 1986.
[46] J. Nyman, G.M. Day, Static and lattice vibrational energy differences between polymorphs, CrystEngComm 17 (2015) 5154–5165.
[47] S.V. Bondarchuk, Impact sensitivity of aryl diazonium chlorides: limitations of molecular and solid-state approach, J. Mol. Graph. Model. 89 (2019) 114–121.
[48] C.P. Brock, J.D. Dunitz, Towards a grammar of crystal packing, Chem. Mater. 6 (1994) 1118–1127.
[49] Q. Zhu, A.R. Oganov, C.W. Glass, H. Stokes, Constrained evolutionary algorithm for structure prediction of molecular crystals: methodology and applications, Acta Crystallogr. B 68 (2012) 215–226.
[50] L.R. Domingo, M. Ríos-Gutiérrez, P. Pérez, Applications of the conceptual density functional theory indices to organic chemistry reactivity, Molecules 21 (2016) 748.
[51] D. Cremer, E. Kraka, A description of the chemical bond in terms of local properties of electron density and energy, Croat. Chem. Acta 57 (1984) 1259–1281.
[52] S.V. Bondarchuk, Significance of crystal habit sphericity in the determination of the impact sensitivity of bistetrazole-based energetic salts, CrystEngComm 20 (2018) 5718–5725.
[53] S.V. Bondarchuk, A unified model of impact sensitivity of metal azides, New J. Chem. 43 (2019) 1459–1468.
[54] S.V. Bondarchuk, Quantification of impact sensitivity based on solid-state derived criteria, J. Phys. Chem. A 122 (2018) 5455–5463.
[55] S.V. Bondarchuk, Impact sensitivity of crystalline phenyl diazonium salts: a first-principles study of solid-state properties determining the phenomenon, Int. J. Quant. Chem. 117 (2017), e25430.
[56] W. Setyawan, S. Curtarolo, High-throughput electronic band structure calculations: challenges and tools, Comput. Mater. Sci. 49 (2010) 299–312.
[57] P. Vannucci, Anisotropic elasticity, in: P. Wriggers, P. Eberhard (Eds.), Lecture Notes in Applied and Computational Mechanics, vol. 85, Springer, Berlin, 2018, p. 426.
[58] E.F.C. Byrd, B.M. Rice, Improved prediction of heats of formation of energetic materials using quantum mechanical calculations, J. Phys. Chem. A 110 (2006) 1005–1013.
[59] The NIST chemistry WebBook. https://webbook.nist.gov/. (Accessed 19 November 2019).
[60] M.J. Kamlet, S.J. Jacobs, Chemistry of detonations. I. A simple method for calculating detonation properties of C-H-N-O explosives, J. Chem. Phys. 48 (1968) 23–35.
[61] S.V. Bondarchuk, N.A. Yefimenko, An algorithm for evaluation of potential hazards in research and development of new energetic materials in terms of their detonation and ballistic profiles, Propellants, Explos. Pyrotech. 43 (2018) 818–824.
[62] A. Burcat, Thermochemical data for combustion calculations, in: W.C. Gardiner Jr. (Ed.), Combustion Chemistry, Springer, Berlin, 1984, pp. 455–473.
[63] S. Gordon, B.J. McBride, Computer Program for Calculation of Complex Chemical Equilibrium Compositions and Applications. I. Analysis, NASA Reference Publication 1311, NASA, Cleveland, OH, 1994.
[64] T. Yu, B. Wu, A theoretical prediction on CN_6O: structure, stability and performance, Inorg. Chem. Front. 2 (2015) 991–1000.
[65] A.M. Hardman, S.S. So, A.E. Mattson, Urea-catalyzed construction of oxazinanes, Org. Biomol. Chem. 11 (2013) 5793–5797.
[66] V.F. Rudchenko, S.M. Ignatov, I.I. Chervin, A.E. Aliev, R.G. Kostyanovsky, Synthesis and properties of 2,3-dimethoxy-1,4,2,3-dioxadiazinane and dialkoxydiazene oxides, Mendeleev Commun. 2 (1992) 50–51.
[67] J.C. Stowell, C.M. Lau, Synthesis and reactions of the first examples of the 1,5,2,4-dioxadiazine ring system: 2,4-Dialkyl-2*H*-1,6,2,4-dioxadiazine-3,6(4*H*)-diones, J. Org. Chem. 51 (1986) 3355–3357.
[68] F. Dubnikova, R. Kosloff, J. Almog, Y. Zeiri, R. Boese, H. Itzhaky, A. Alt, E. Keinan, Decomposition of triacetone triperoxide is an entropic explosion, J. Am. Chem. Soc. 127 (2005) 1146–1159.